Accepted Manuscript

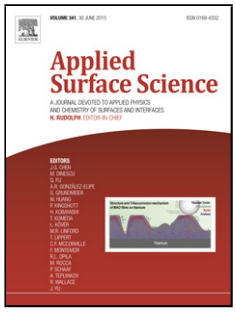

Title: Cyanate ester resin filled with graphene nanosheets and $CoFe_2O_4$-reduced graphene oxide nanohybrids as a microwave absorber

Author: Fang Ren Guangming Zhu Penggang Ren Kun Wang Xiaoping Cui Xiaogang Yan

PII: S0169-4332(15)01220-9
DOI: http://dx.doi.org/doi:10.1016/j.apsusc.2015.05.101
Reference: APSUSC 30427

To appear in: *APSUSC*

Received date: 26-3-2015
Revised date: 28-4-2015
Accepted date: 17-5-2015

Please cite this article as: Cyanate ester resin filled with graphene nanosheets and $CoFe_2O_4$-reduced graphene oxide nanohybrids as a microwave absorber, *Applied Surface Science* (2015), http://dx.doi.org/10.1016/j.apsusc.2015.05.101

Cyanate ester resin filled with graphene nanosheets and $CoFe_2O_4$-reduced graphene oxide nanohybrids as a microwave absorber

Fang Ren[a] Guangming Zhu [a] Penggang Ren[b] Kun Wang [a] Xiaoping Cui[a] XiaogangYan[a]

a. Department of Applied Chemistry, Northwestern Polytechnical University, Xi'an, Shaanxi 710129, P.R. China

b. The Faculty of Printing and Packaging Engineering, Xi'an University of Technology, Xi'an Shaanxi 710048, P.R. China

Contact address: Dr. Guangming Zhu

Department of Applied Chemistry

Northwestern Polytechnical University

Xi'an, Shaanxi 710129

P. R. China

E-mail: gmzhu@nwpu.edu.cn

Highlights

1. Novel composites composed of $CoFe_2O_4$ spheres and reduced graphene oxide (RGO) were synthesized by using a facile hydrothermal route in combination with calcination at 550^oC.
2. GNSs/RGO-$CoFe_2O_4$nanohybrid/Cyanate ester resin composites exhibited excellent electromagnetic absorption properties and wide absorption bandwidth.
3. Too high permittivity of the composites is harmful to the impedance match and results in strong reflection and weak absorption.

Abstract: Novel composites composed of $CoFe_2O_4$ spheres and reduced graphene oxide (RGO) were synthesized by using a facile hydrothermal route in combination with calcination at 550^oC. A series of characterization results indicate that the as-prepared $CoFe_2O_4$ spheres with relatively uniform sizes are homogeneously distributed on RGO layers. As absorbing materials, absorption properties of the graphene sheets (GNSs)/RGO-$CoFe_2O_4$ nanohybrid/Cyanate ester resin (CE) composites were investigated in the measured microwave range of X-band (8.2-12.4 GHz). It can be found that the maximum reflection loss of the GNSs/RGO-$CoFe_2O_4$ nanohybrid/CE composites can reach -21.8 dB at 11.8 GHz with a thickness of 1.25 mm, and the frequency bandwidth less than -10 dB is from 9.6 to 12.4 GHz. The enhanced electromagnetic absorption property of the composites was attributed to the better impedance matching. While, when the GNSs loading is 5 wt%, high permittivity of the composites is harmful to the impedance match and results in strong reflection and weak absorption. Therefore, the GNSs/RGO-$CoFe_2O_4$ nanohybrid/CE composites, with excellent electromagnetic absorption properties and wide absorption bandwidth, can be

obtained via adjusting the filler content to meet wide applications in the aerospace industry.

Keywords: $CoFe_2O_4$ sphere; Reduced graphene oxide; Cyanate ester resin; Graphene sheets; GNSs/RGO-$CoFe_2O_4$/CE composites; Wave absorption properties

1. Introduction

Electromagnetic interference has become a pollution problem due to the extensive utilization of electronic devices and communication facilities in industry, commerce, and military affairs [1]. A good method to solve the problem is using microwave absorption materials to absorb those unwanted electromagnetic energies and transform electromagnetic energy into thermal energy or make microwaves dissipated by interference [2-3]. However, traditional ferrites have narrow wave absorbing band and poor flexibility, combined with their high density and poor environmental stability which restrict their wide applications as microwave absorbents [4-6]. An "ideal" electromagnetic wave absorbing material should exhibit low density, tiny thickness, strong wave absorption and broad bandwidth simultaneously [7-8]. Graphene, a novel carbon nanomaterial with a unique two-dimensional conjugated structure, exhibits a high surface area, superior electrical conductivity and strong mechanical stability, and therefore has attracted increasing attention for its potential applications in electronics, catalysis, sensors, and energy-storage devices [9-13]. Moreover, the high dielectric loss and low density make graphene a promising material for electromagnetic wave absorption properties. However, the maximum absorption value of pure graphene is only -6.9 dB, which is unsuitable for practical applications [14]. Recently, considering the outstanding properties of graphene, decorating graphene sheets (GNSs) with magnetic nanoparticles, would obtain a good absorption of the reported GNSs/magnetic particle-filled composite, as shown in Table. 1.

Absorber and content	preparation method	Thickness (mm)	Bandwidth (RL<-10 dB)(GHz)	RL_{min}(dB)	Refs.
30wt% (graphene–Ni)	Microwave-assisted heating approach	2	12-18	-42	[15]
5wt% (3Dgraphene@CNTs)	One-pot pyrolysis strategy	3	7.1-10.4	-44.6	[16]
50 wt% (FeCo/graphene)	one-pot polyol followed by chemical conversion	2.5	3.4-18	-40.2	[17]
80wt% ($BaFe_{12}O_{19}$/RGO)	Wet chemical method and hot-pressing approach	2	~8.4-17	-32	[18]
30wt% (GO@FeCoB)	Co-precipitation	2	10-12.4	-22.24	[19]
10wt% (graphene–CdS)	Facile hydrothermal approach	3.3	5.2-18	-48.4	[20]
10wt% (Fe_3O_4/graphene)	An atomic layer deposition (ALD) method	1.4	12.4-16.9	-46.4	[21]
10wt% (3D graphene–Fe_3O_4)	Direct hydrothermal grafting method	3	9.2-15	-23	[22]
70wt% ($CoFe_2O_4$/graphene)	Facile one-pot polyol route	2.5	5.4-18	-36.4	[23]
20 wt% (3Dγ-Fe_2O_3/graphen)	Seed-assisted method	4.92	~4-10	-64.1	[24]
70wt%($NiFe_2O_4$ nanorod/graphene)	Facile one-step hydrothermal process	2	13.6-18	-29.2	[25]

These composites exhibit excellent wave absorption properties, which is possibly resulted from the synergistic effect of their high magnetic loss from magnetic nanomaterials and electric loss from light-weight graphene, leading to well impedance matching and high-performance electromagnetic wave attenuation [25]. However, most of these materials use wax as the matrix, and the weight in the matrix is more, which restrict these applications in many fields. More recently, inorganic–organic nanocomposites showed enhanced microwave absorption abilities with promising applications [26]. The existence of a synergic effect between inorganic nanofillers and organic polymer matrix could distinctly enhance the wave absorption of the nanocomposite [27].

Conductive polymer composites (CPCs) containing electrical nanofillers are particularly desirable in the areas of aircraft, spacecraft, energy storage techniques, and automobiles, based on their own superiorities, such as their lightweight, low cost, good processibility, and tunable

conductivities over a wide range [28-31]. CPCs based on graphene have been used for improved mechanical, thermal, electrical, gas barrier and microwave absorbing properties of polymers [32-34].

In order to expand the range of applications, we use cyanate ester (CE) instead of wax as a matrix. CE resin is superior to conventional epoxy as the next-generation thermosetting polymer matrix. The very low moisture absorption, good mechanical properties, good radiation resistance, long pot-life and cost-effective property make it suitable for use in many areas, such as electric packaging for microelectronic industries, matrix resins for aerospace applications and structural composites [35]. In the aerospace industry, CE based composites are often used for engine cowlings and thrust reversers and for structural skins [36-38]. Herein, RGO-$CoFe_2O_4$ nanohybrid were fabricated using a facile in situ solvothermal route in the presence of polyvinyl pyrrolidone (PVP), followed by calcination, and combining using GNSs, we first investigated their wave absorption properties with CE.

2. Materials and methods

2.1 Materials

GO was synthesized by the modified Hummers method [39]. Graphene nanosheets (average thickness<30nm, specific surface area～60m^2/g) was supplied by Xiamen Knano Graphene Co.,Ltd. Bisphenol A dicyanate ester (BADCy) was obtained from Shengda curatorial Co., Ltd. (Zhejiang, China). Bisphenol-A based epoxy (Epoxy E-51) with epoxide equivalent weight 184-200g/equiv, was purchased from Lanxing resin Co.,Ltd (Wuxi, China). All other reagents and solvents were purchased from Beijing Chemicals. All chemicals used in our experiments were of

reagent grade and used without further purification.

2.2 Synthesis of RGO-$CoFe_2O_4$ composites

The detailed process is described as follows: 0.15 g of PVP was dissolved in 20 mL of deionized water with magnetic stirring. After complete dissolution, 0.404 g of $Fe(NO_3)_3 \cdot 9H_2O$ and 0.145 g of $Co(NO_3)_2 \cdot 6H_2O$ were added to the above solution. Then, 40 mL of GO (3.75 mg ml^{-1}) was added to the solution mixture and dispersed by ultrasonication for 30 min. Subsequently, the mixture was transferred to a 100 mL Teflon-lined autoclave and 0.12 g of urea was placed in the internal tray. The autoclave was sealed and maintained at 180 ^oC for 12 h, then naturally cooled to room temperature. The precipitate was collected, washed, and dried under vacuum at 60 ^oC for 12 h. RGO-$CoFe_2O_4$ nanohybrids were obtained by annealing the as obtained precipitate at 550 ^oC under argon protection for 1 h.

2.3 Synthesis of GNSs/RGO-$CoFe_2O_4$ /CE composites

All of GNSs/RGO-$CoFe_2O_4$/CE resin composites with different contents of GNSs (1-5 wt%) and constant loadings (10wt%) of RGO-$CoFe_2O_4$ were prepared by solution blending. A typical procedure of GNSs/RGO-$CoFe_2O_4$/CE composite with 5wt% of GNSs and 10wt% of RGO-$CoFe_2O_4$ is as follows: A solution of 0.167g of RGO-$CoFe_2O_4$ and 0.08g GNSs in 20ml acetone was sonicated for 1h. After 1.5g of the CE prepolymer (1.2g BADCy and 0.3g E-51 were mixed at 100^oC and stirred for 30 min, which the resultant liquid was defined as CE prepolymer.) was added into GNSs/RGO-$CoFe_2O_4$/acetone solution and dispersed ultrasonically for 30 min. The acetone was then evaporated off by heating the mixtures in a temperature controlled oil bath pot at 80^oC while stirring at a speed of 300 rpm for 2 h to ensure removal of residual solvent and

then the mixture were placed in a vacuum oven to remove entrapped air at 100°C for 2h. After that, the mixture was cast into a mold for curing and postcuring with the sequence 120°C/1h+150°C/2h+180°C/2h+200°C/2h. And all the process can be express as follow Fig 1.

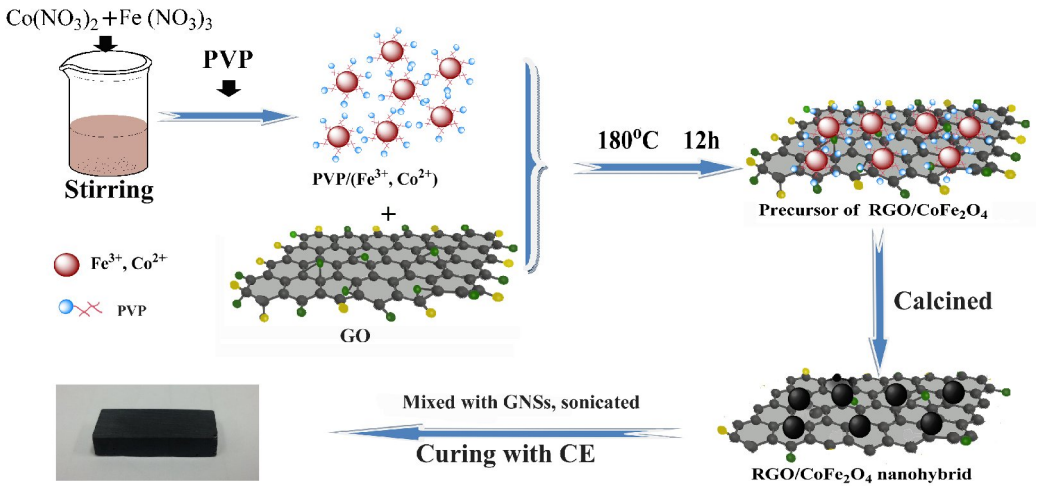

Fig. 1. Schematic for the process of GNSs/RGO-$CoFe_2O_4$/CE composites.

2.4 Characterization

X-ray diffraction (XRD) patterns were recorded in the range of 2θ = 5°-85° using an X-ray diffractometer (modelD/max-2500system, Rigaku) with Cu Ka radiation (k = 1.54056 Å) at 30 kV and 15 mA. Fourier transform infrared (FTIR) spectra for the GO and RGO-$CoFe_2O_4$ nanohybrid were recorded between 500 and 4000 cm^{-1} with a resolution of 2 cm^{-1} on an IS10 Infrared Spectrometer (USA). Transmission electron microscopy (TEM) was performed with a Tecnai G^2 F20S-TWIN electron microscope. Stable dispersion of the GO and RGO-$CoFe_2O_4$ nanohybrid (dispersed in ethanol) were prepared by ultrasonic treatment. A drop of stable dispersion was placed on a copper grid and then dried before it was transferred to the sample chamber. Scanning electron microscopy (SEM) images were achieved by a FEI Quanta 250 field-emission gun

environmental scanning electron microscope at 10 kV. The chemical states were investigated by X-ray photoelectron spectroscopy (XPS, AXIS Ultra DLD). The complex permittivity of the composites was measured using the wave-guide method in the frequency range of 8.2-12.4 GHz by a network analyzer (Agilent technologies E8362B: 10 MHz-20 GHz).

3. Results and discussion

3.1 The morphology of RGO-$CoFe_2O_4$ nanohybrid and GNSs filled composites.

XRD measurements were employed to investigate the phase and structure of the synthesized samples. Fig. 2a shows the XRD profile of the GNSs, GO and RGO-$CoFe_2O_4$ nanohybrid. GO exhibits a strong diffraction peak at 10.1^o, corresponding to the (001) reflection with an interlayer spacing of 0.8864 nm, which is larger than that of graphite (0.34 nm). The enhancement of interlayer spacing is due to the formation of oxygenic functional groups between the graphite layers [40]. GNSs powders present no visible peak. Although this does not necessarily mean that all stacking is lost, it does indicate the disordered stacking structure of the GNSs powders [41-42]. For the RGO-$CoFe_2O_4$ hybrids, the diffraction peaks at $2\theta = 30.2^o$, 35.6^o, 47.5^o, 43.3^o, 57.4^o, 62.8^o and 75.1^o can be respectively indexed to the (220), (311), (400), (422), (511), (440) and (533) crystal planes of the pure spinel $CoFe_2O_4$ (JCPDS no. 00-022-1086) suggesting the formation of $CoFe_2O_4$ nanocrystals.

Fig. 2b shows FTIR spectra of the GNSs, GO and RGO-$CoFe_2O_4$ nanohybrid. GNSs show no obvious absorption in the infrared range. The characteristic bands of the GO were observed at 3421 cm^{-1}, 1733 cm^{-1}, 1623 cm^{-1}, 1097 cm^{-1}, which are due to the vibration and deformation bands of O–H and C=O stretching vibrations from carbonyl groups, C=C configurable vibrations from

the aromatic zooms, C–OH stretching vibrations, C–O vibrations from epoxy groups and C–O vibrations from alkoxy groups, respectively [43]. However, most of the peaks related to the oxygen containing functional groups vanish or weaken in the FTIR spectrum of RGO-$CoFe_2O_4$ nanohybrid, revealing that GO were reduction in the process of calcinations. New peaks that appear at 587cm^{-1} in RGO-$CoFe_2O_4$ nanohybrid could be ascribed to lattice absorption of Fe–O, further confirming the existence of $CoFe_2O_4$ [44].

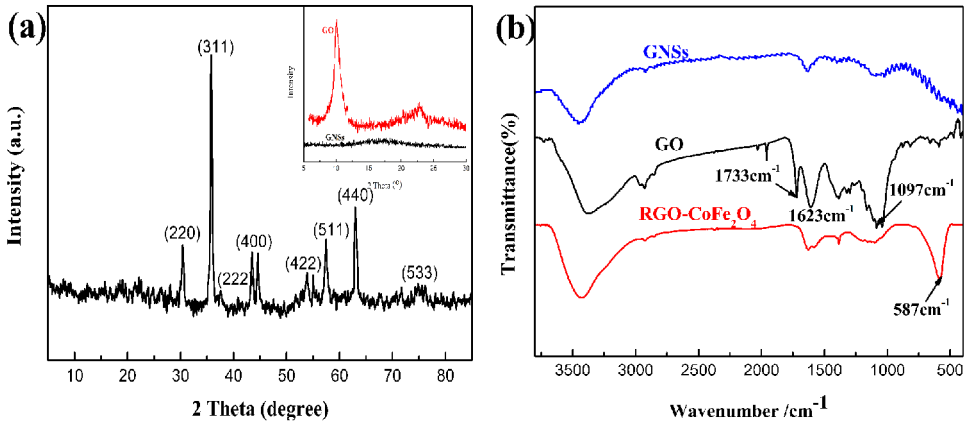

Fig. 2. (a) XRD patterns and (b) FTIR spectra of GNSs, GO and RGO-$CoFe_2O_4$ nanohybrid.

The chemical composition of the samples was also characterized by XPS spectra (Fig. 3). In the wide scan XPS spectrum (Fig. 3a-b), several sharp peaks with the binding energy of 285, 530, 711 and 780 eV, were attributed to C 1s, O 1s, Fe 2p and Co 2p, respectively, indicating the existence of C, O, Fe and Co elements in the RGO-$CoFe_2O_4$ nanohybrid. Compared with GO, the oxygen content of RGO-$CoFe_2O_4$ nanohybrid decreased rapidly, suggesting a remarkable reduction after the hydrothermal reaction and the process of calcinations (Fig. 3d). The Fe 2p spectrum (Fig. 3e) exhibits two peaks at 710.9 and 724.5 eV, corresponding to Fe 2p3/2 and Fe 2p1/2, respectively. In Fig. 3f, the Co2p3/2 signal appeared at 781.0 eV, and the peak at 797.1 eV was ascribed to the Co2p1/2 level. These results suggest the formation of $CoFe_2O_4$ nanocrystals.

The morphology and structure of the RGO-$CoFe_2O_4$ nanohybrid were investigated by TEM and

SEM. It can be seen from Fig. 4a and b that RGO supports are obviously decorated by plenty of spheres with a diameter of about 30-40 nm. Besides, the transparent thin morphology demonstrates that the RGO is composed of a few layers. The high-resolution TEM (HRTEM) image of $CoFe_2O_4$ nanocrystals (Fig. 4d) shows clear lattice fringes with an interplanar distance of 0.49 nm, which can be assigned to the (111) plane of $CoFe_2O_4$. The selected area electron diffraction (SAED) pattern of RGO/$CoFe_2O_4$ hybrids (Fig. 4d) shows the standard ring patterns resulted from the cubic spinel structure of $CoFe_2O_4$, which is consistent with the XRD result. All the above analyses confirm the successful self-assembly of $CoFe_2O_4$ spheres on the whole large graphene sheets.

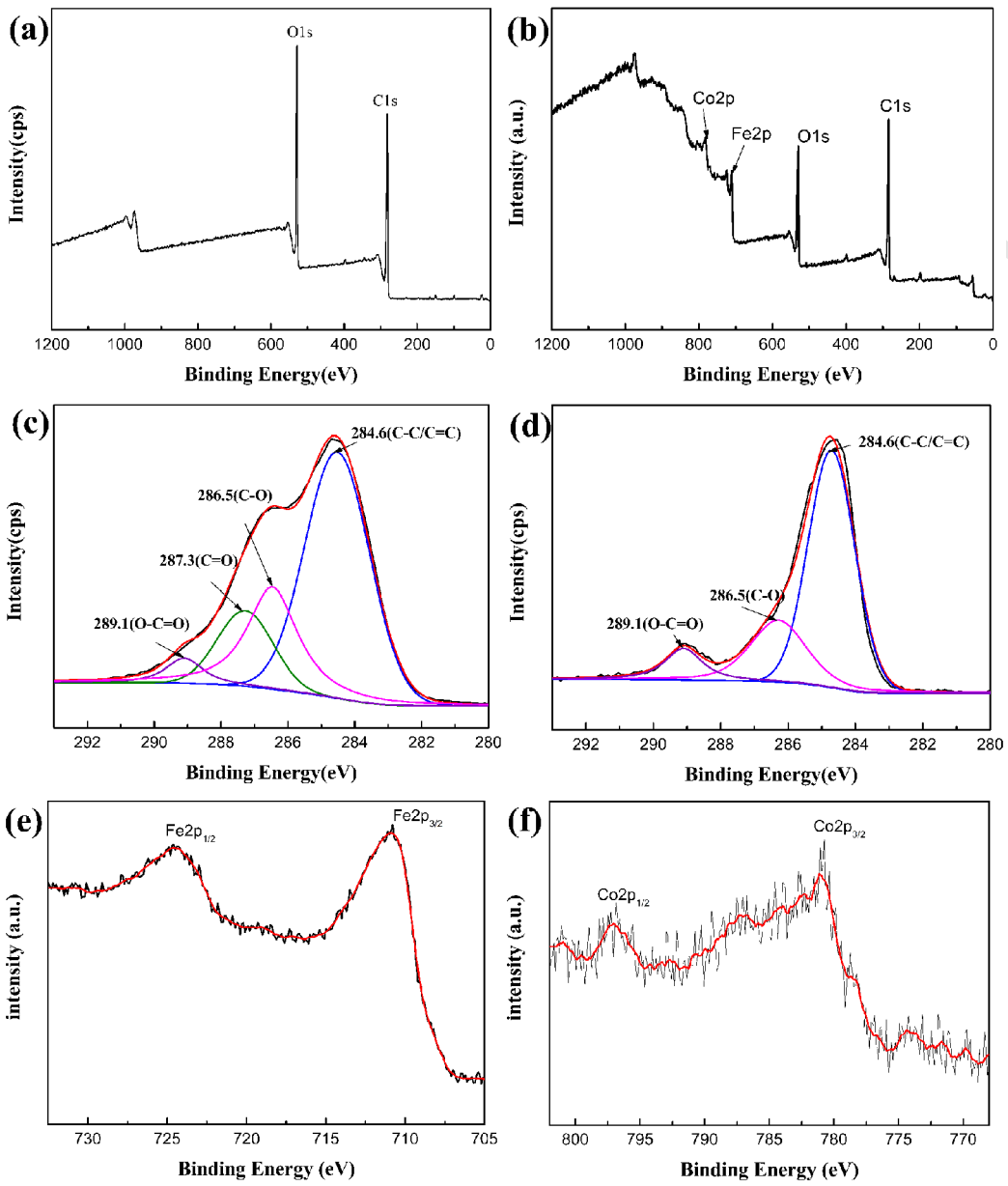

Fig. 3. XPS spectra: wide scan of (a) GO and (b) RGO-$CoFe_2O_4$ nanohybrid, (c) C 1s spectra of GO and (d) C 1s spectra of RGO-$CoFe_2O_4$ nanohybrid, (e) Co2p and (f) Fe2p spectra of RGO-$CoFe_2O_4$ nanohybrids.

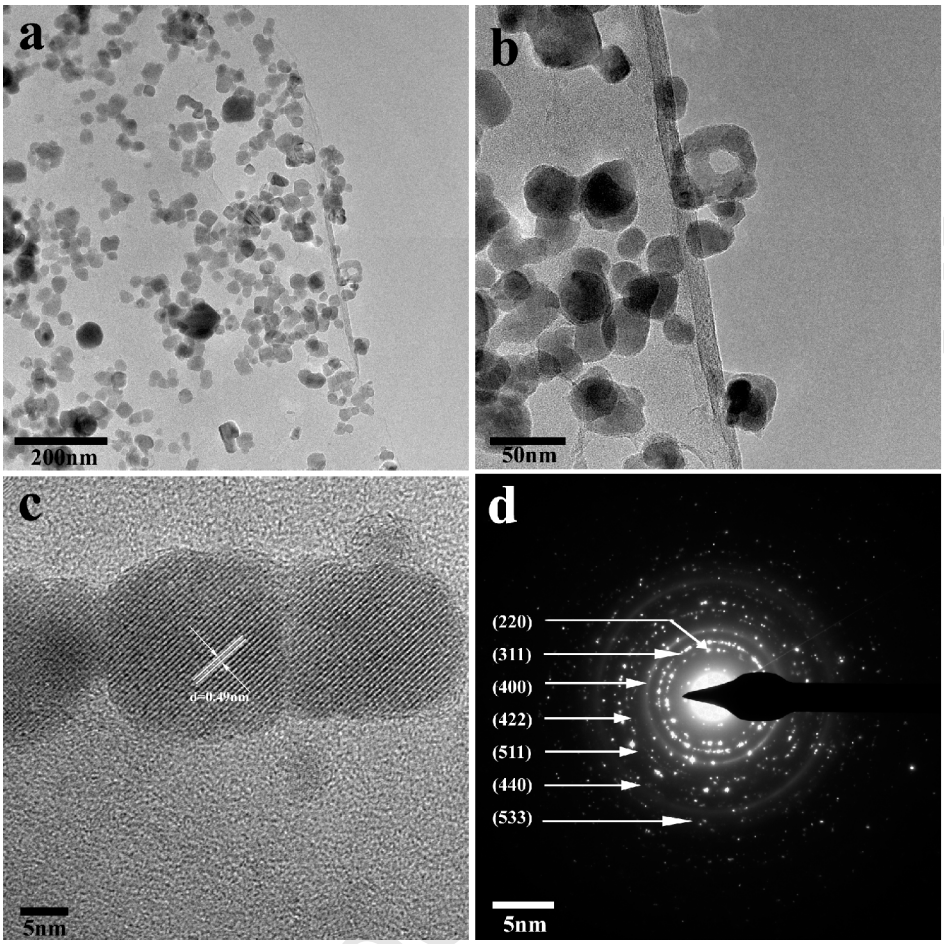

Fig. 4. TEM images of RGO-$CoFe_2O_4$ nanohybrid with different magnifications (a) and (b), high-resolution TEM image of RGO-$CoFe_2O_4$ (c), selected area electron diffraction (SAED) pattern of RGO-$CoFe_2O_4$ (d)

It is clear that two dimensional GNSs present a lamellar structure of alternating plates and $CoFe_2O_4$ sphere disperse uniformly on the surface of RGO, as showed in Fig. 5a and b. The as-prepared RGO-$CoFe_2O_4$ hybrids exhibit crinkled and rough textures, which are associated with the presence of flexible and thin RGO sheets. Fig. 5c-d clearly showed GNSs and RGO-$CoFe_2O_4$ were well–dispersed in the resin matrix. The GNSs and RGO-$CoFe_2O_4$ were exposed to ultrasound in acetone and then stirring the mixture intensely. This approach can lead to a dramatic improvement of GNSs dispersion throughout the matrix [45].

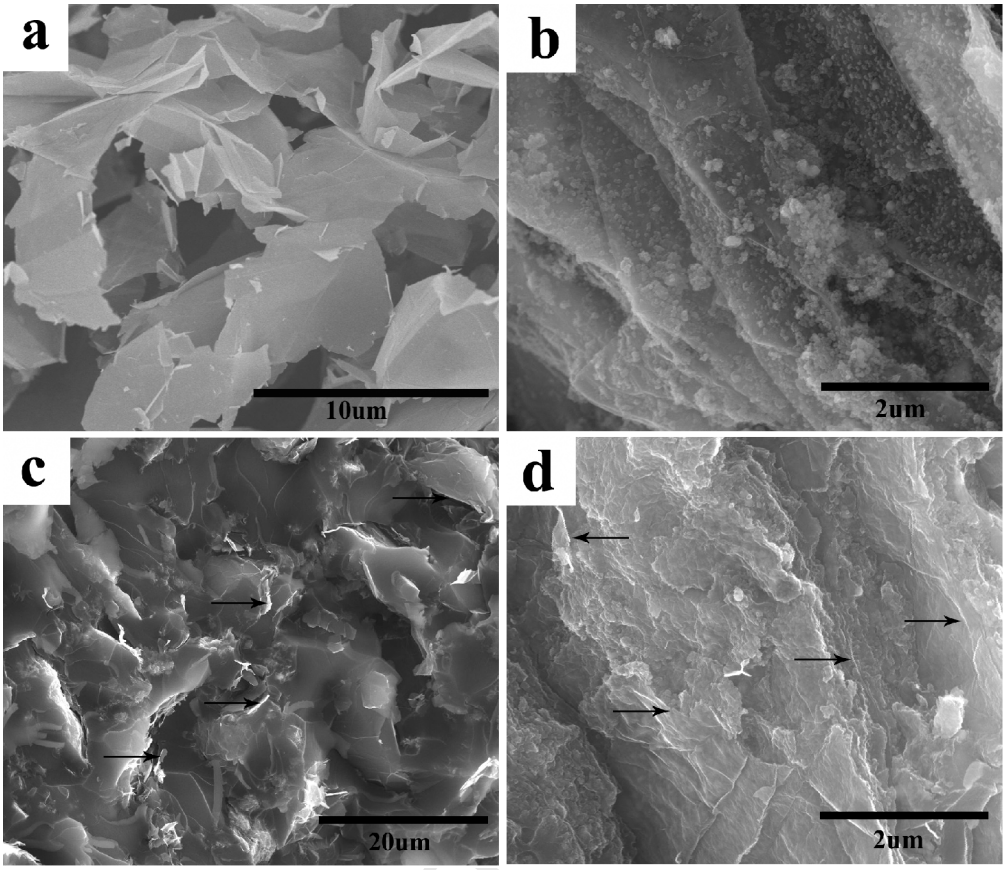

Fig. 5. SEM images of the (a) GNSs (b) RGO-$CoFe_2O_4$ nanohybrid (c, d) GNSs/RGO-$CoFe_2O_4$/CE composites (the black arrows for the GNSs).

3.2 Electromagnetic parameters and absorbing performance.

It is believed that the complex permittivity and permeability of the absorbers determine the microwave absorption properties of the absorbers filled composites. In order to evaluate the microwave electromagnetic of GNSs/RGO-$CoFe_2O_4$/CE composites, we measured the complex permittivity and permeability of the composites in the frequency range of 8.2–12.4 GHz. Fig. 6 shows the complex permittivity spectra of the composites containing different contents of GNSs and constant loadings of RGO-$CoFe_2O_4$. It is clearly that both the value and frequency dependent of the complex permittivity changed with the absorber content. With increasing the GNSs content,

both real (ε') and imaginary (ε'') part of the complex permittivity increased in the frequency range of 8.2-12.4GHz，but decreased with increasing frequency. These because the dielectric loss mechanisms of the conductive particle filled insulation resin composites were mainly caused by deflection of dipole and interfacial polarization [46]. The ε' of composites depends on the configuration and internal fractal structure, which is proportional to the quantity of charge stored on the surface when the composites under an applied electric field. The higher content of two dimensional GNSs incorporated into the resin, the more GNSs/RGO-$CoFe_2O_4$/resin interfaces formed, which certainly increased the ε' of such absorber. On the other hand, the main term affecting the ε'' is the interfacial polarization and its associated relaxation while the conductivity term plays a secondary role when a sample is filled with low content of GNSs. When the content of GNSs increased, the electrical conductivity also can affect the values of the ε'' of such composites. The higher electrical conductivity, the higher values of ε'', as showed in the Fig. 6b. Thus, it is reasonable that the higher complex permittivity (both the ε' and ε'') can be obtained when the composites filled with higher content of GNSs. Furthermore, because the interfacial polarization can be more easily induced at lower frequency and the production of displacement current significantly lags behind the build-up potential as the frequency increased. Thus, it is reasonable that both ε' and ε'' decreased with increasing frequency and exhibited a visible frequency-dependent dielectric response [47-48]. The complex permeability spectra of the composites containing different GNSs and constant RGO-$CoFe_2O_4$ are presented in Fig. 6c and d. It can be found that the complex permeability increased slightly as the GNSs content increased when under the same RGO-$CoFe_2O_4$ content. The GNSs/RGO-$CoFe_2O_4$/polymer interfacial features are expected to have a profound impact not only on the interactions between the $CoFe_2O_4$

particles and RGO, GNSs and the surrounding matrix but also the electrically controlled exchange bias and magnetocrystalline anisotropy in the specific case of $CoFe_2O_4$ particles [46]. Therefore, the slightly increased of complex permeability are believed due to the interactions between the GNSs and RGO-$CoFe_2O_4$ in the CE resin matrix, as the GNSs content increased when under the same RGO-$CoFe_2O_4$ content.

The loss tangent commonly used to describe dielectric loss, is calculated based on the measured complex permittivity of such composite. The dielectric loss ($\tan\delta_\varepsilon = \varepsilon''/\varepsilon'$) and magnetic loss ($\tan\delta_\mu = \mu''/\mu'$) depended on the content of the fillers and frequency, as shown in Fig. 6e and f. Further, it is observed that the values of $\tan\delta_\varepsilon$ and $\tan\delta_\mu$ showed some fluctuation in the measured frequency range, and $\tan\delta_\varepsilon$ increased with increasing the GNSs loadings. The flake structure of the GNSs is beneficial to the improved dielectric properties [49]. Furthermore, the dielectric loss mechanism of the GNSs is mainly attributed to the interfacial polarization. Some defects on the surface of GNSs can act as polarization centers under the altering electromagnetic field and attenuate electromagnetic waves, resulting in a profound effect on the loss of microwaves. In addition, there are residual oxygen containing chemical bonds such as C–O, C=O on the RGO, which enhance dielectric loss [50].

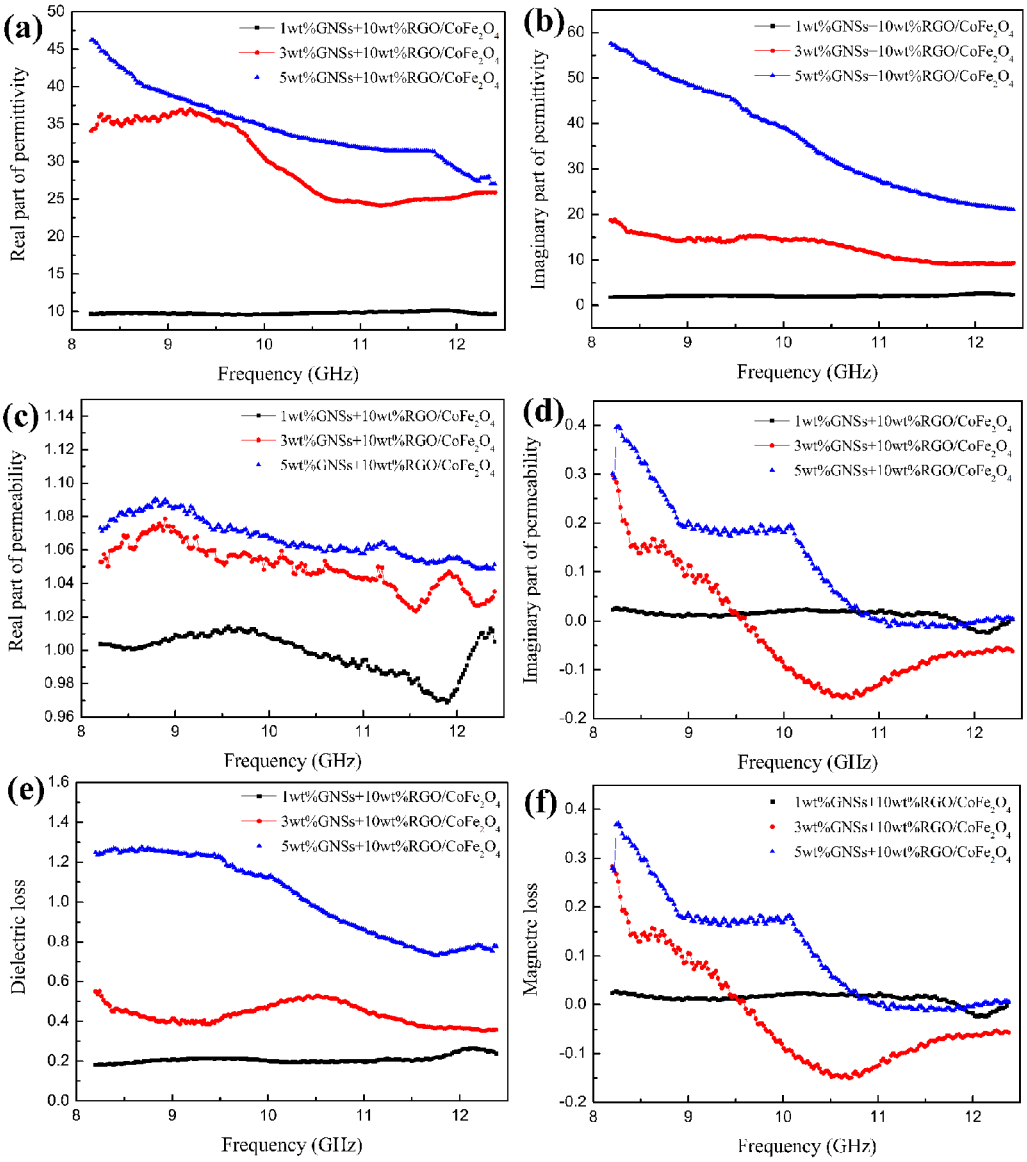

Fig. 6. Frequency dependence of the (a) real and (b) imaginary parts of the complex permittivity, the (c) real and (d) imaginary parts of the complex permeability, and the corresponding (e) dielectric and (f) magnetic loss tangents of the sample.

The theoretical reflection loss values of the composites can be obtained according to the transmission line theory [51].The reflection loss for a single-layer absorber is given by following relation:

$$RL(dB) = 20\log\left|\left(Z_{in} - Z_0\right)\Big/\left(Z_{in} + Z_0\right)\right| \quad (1)$$

Where the input impedance of the absorber Z_{in} is given

$$Z_{in} = Z_0 \sqrt{\frac{\mu_r}{\varepsilon_r}} \tanh\left[j \frac{2\pi f d}{c} \sqrt{\mu_r \varepsilon_r} \right] \quad (2)$$

Where Z_0 is the impendency of the free space; ε_r and μ_r are the relative permittivity and permeability of the absorber; c is the velocity of light in free space; f is the frequency of the electromagnetic wave; d is the thickness of the absorber. Thus, the reflectance of an absorber on metal surface is determined by the relative permittivity and permeability at a given frequency as well as the thickness of microwave absorbing materials. Fig. 7 shows the reflection loss of composites containing different content of GNSs with the different thickness. It can be concluded that the reflection loss of the GNSs/RGO-$CoFe_2O_4$/CE composites depended on electromagnetic frequency, GNSs, and/or RGO-$CoFe_2O_4$ content and composites thickness. Simultaneously, the frequencies of the largest absorption values shifted to lower frequency ranges with increasing the composite thicknesses. Furthermore, the largest absorption values were obtained at thinner thicknesses with increasing the GNSs content. However, too larger complex permittivity, especially in the high frequency range, will decrease the microwave absorption of such absorber (Fig. 7c). Based on some previous reports, the enhancement in the dielectric constant can be explained according to the percolation theory [52]. In our GNSs/RGO-$CoFe_2O_4$/CE system, the conductive GNSs network enhances the electrical conductivity of the composite and this leads to a high leakage current, which may cause damage to the wave-absorption of materials [53]. Another important concept relating to microwave absorption is impedance match characteristic. High permittivity of absorber is harmful to the impedance match and results in strong reflection and weak absorption [54]. For example, when the loading of the GNSs in CE is 1wt%, 3wt%, 5wt%, the maximum reflection loss can be achieved to -12.4dB at 2mm, -21.8 dB at 1.25mm, -5.7dB at

1mm, respectively. Meanwhile, the reflection loss values of the composites filled with 3wt% GNSs below -5dB obtained in the frequency range of 8.2-12.4 GHz with a thickness of 1.25 mm, below -10 dB obtained in the frequency range of 9.6-12.4 GHz. These results indicate that GNSs/RGO-$CoFe_2O_4$ filled CE composites with wider microwave absorption bandwidth and/or thinner thicknesses.

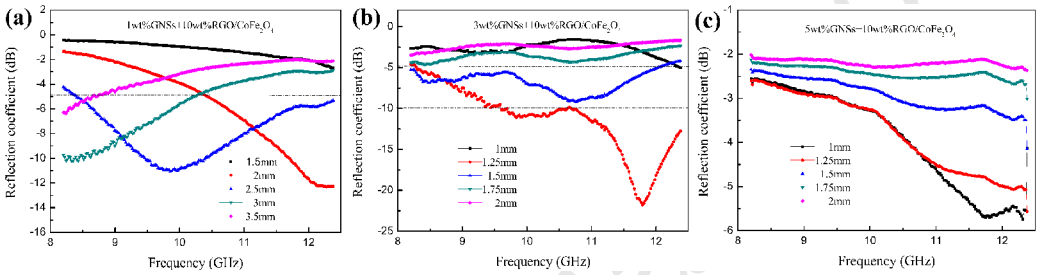

Fig. 7. Frequency dependence of the RL of composite containing constant loading of 10wt%RGO-$CoFe_2O_4$ and different contents of GNSs at different thickness: (a) 1wt%, (b) 3wt%, and (c) 5wt%.

4. conclusion

RGO-$CoFe_2O_4$ nanohybrids were fabricated using a facile in situ solvothermal route in the presence of PVP, followed by calcination. And combining using GNSs, we first investigated their wave absorption properties with CE. Among the composites with different loading of GNSs (1, 3, 5wt%) and 10wt% RGO-$CoFe_2O_4$ nanohybrid, the composite with a 3wt% GNSs loading shows the best absorption peak value (-21.8dB with 1.25mm). Reflection loss values less than –10 dB (more than 90% absorption) were obtained in the measured frequency range of 9.6-12.4 GHz with a thickness of 1.25 mm. The main contribution for the microwave absorption comes from the dielectric loss rather than the magnetic loss. While, when the GNSs loading is 5 wt%, high permittivity of the composites is harmful to the impedance match and results in strong reflection

and weak absorption. These results indicate that moderate GNSs/RGO-$CoFe_2O_4$ filled composites may have great potential for broad bandwidth microwave absorbing applications.

Acknowledgements

The authors thank for the financial supports by the National Foundation of China (Grant No. 51273161) and are grateful to Dr. Yuchang Qing at State Key Laboratory of Solidification Processing for the complex permittivity measurements.

References

[1] J.W. Liu, R.C. Che, H.J. Chen, F. Zhang, F. Xia, Q.S. Wu, M. Wang, Microwave absorption enhancement of multifunctional composite microspheres with spinel Fe_3O_4 cores and anatase TiO_2 shells, Small 8 (2012) 1214–1221.

[2] M. Zong, Y. Huang, X. Ding, N. Zhang, C.H. Qu, Y.L. Wang, One-step hydrothermal synthesis and microwave electromagnetic properties of RGO/$NiFe_2O_4$ composite, Ceramics International 40 (2014) 6821–6828.

[3] X.H. Guo, Y.H. Deng, D. Gu, R.C. Che, D.Y. Zhao, Synthesis and microwave absorption of uniform hematite nanoparticles and their core-shell mesoporous silica nanocomposites, Journal of Materials Chemistry 19 (2009) 6706-6712.

[4] W.J. Kim, S.S. Kim, Preparation of Ag-coated hollow microspheres via electroless plating for application in lightweight microwave absorbers, Applied Surface Science 329 (2015) 219-222.

[5] K. Khan, Microwave Absorption Properties of Radar Absorbing Nanosized Cobalt Ferrites for High Frequency Applications, Journal of Superconductivity and Novel Magnetism 27 (2014) 453-461.

[6] V. Sunny, P. Kurian, P. Mohanan, P.A. Joy, M.R. Anantharaman, A flexible microwave absorber based on nickel ferrite nanocomposite, Journal of Alloys and Compounds 489 (2010) 297-303.

[7] J.L. Guo, H. Wu, X.P. Liao, B. Shi, Facile synthesis of size-controlled silver nanoparticles using plant tannin grafted collagen fiber as reductant and stabilizer for microwave absorption application in the whole Ku band, The Journal of Physical Chemistry C 115 (2011) 23688-23694.

[8] L. Kong, X.W. Yin, Y.J. Zhang, X.Y. Yuan, Q. Li, F. Ye, L.F. Cheng, L.T. Zhang, Electromagnetic wave absorption properties of reduced graphene oxide modified by maghemite colloidal nanoparticle clusters, The Journal of Physical Chemistry C 117 (2013) 19701-19711.

[9] S. Myung, J. Park, H. Lee, K.S. Kim, S. Hong, Ambipolar memory devices based on reduced graphene oxide and nanoparticles, Advanced Materials 22 (2010) 2045-2049..

[10] X.T. Jia, Campos-Delgado J, Terrones M, Meunier V, M.S. Dresselhaus, Graphene edges: a review of their fabrication and characterization, Nanoscale 3 (2011) 86-95.

[11] S.M. Li, B. Wang, J.H. Liu, M. Yu, In situ one-step synthesis of $CoFe_2O_4$/graphene nanocomposites as high-performance anode for lithium-ion batteries, Electrochimica Acta 129 (2014) 33-39.

[12] F. Ren, G.M. Zhu, Y.K. Wang, X.P. Cui, Microwave absorbing properties of graphene nanosheets/epoxy-cyanate ester resins composites, Journal of Polymer Research 21 (2014) 1-7.

[13] P.G. Ren, D.X. Yan, X. Ji, T. Chen, Z.M. Li, Temperature dependence of graphene oxide

reduced by hydrazine hydrate, Nanotechnology 22 (2011) 055705.

[14] C. Wang, X.J. Han, P. Xu, X.L. Zhang, Y.C. Du, S.R. Hu, J.Y. Wang, X.H. Wang, The electromagnetic property of chemically reduced graphene oxide and its application as microwave absorbing material, Applied Physics Letters 98 (2011) 072906.

[15] Z. Zhu, X. Sun, G. Li, et al. Microwave-assisted synthesis of graphene–Ni composites with enhanced microwave absorption properties in Ku-band, Journal of Magnetism and Magnetic Materials, 2015, (377) 95-103.

[16] L. Wang, Y. Huang, C. Li, et al. A facile one-pot method to synthesize a three-dimensional graphene@ carbon nanotube composite as a high-efficiency microwave absorber, Physical Chemistry Chemical Physics, 17 (2015) 2228-2234.

[17] X.H Li, J. Feng, Y. Du, et al. One-pot synthesis of $CoFe_2O_4$/graphene oxide hybrids and their conversion into FeCo/graphene hybrids for lightweight and highly efficient microwave absorber, Journal of Materials Chemistry A 3 (2015) 5535-5546.

[18] H.C He, F.F Luo, N. Qian, et al. Improved microwave absorption and electromagnetic properties of $BaFe_{12}O_{19}$-poly (vinylidene fluoride) composites by incorporating reduced graphene oxides, Journal of Applied Physics 117 (2015) 085502.

[19] S. Das, G.C. Nayak, S.K. Sahu, et al. Development of FeCoB/Graphene Oxide based microwave absorbing materials for X-Band region, Journal of Magnetism and Magnetic Materials 384 (2015) 224-228.

[20] D.D. Zhang, D.L. Zhao, J.M. Zhang, et al. Microwave absorbing property and complex permittivity and permeability of graphene–CdS nanocomposite, Journal of Alloys and Compounds 589 (2014) 378-383.

[21] G.Z Wang, Z. Gao, G.P. Wan, et al. High densities of magnetic nanoparticles supported on graphene fabricated by atomic layer deposition and their use as efficient synergistic

microwave absorbers, Nano Research, 7 (2014) 704-716.

[22] C.G. Hu, Z.Y. Mou, G.W. Lu, et al. 3D graphene-Fe_3O_4 nanocomposites with high-performance microwave absorption, Physical Chemistry Chemical Physics 15 (2013) 13038-13043.

[23] X.H. Li, J. Feng, H. Zhu, C.H. Qu, J.T. Bai, X.L. Zheng Sandwich-like graphene nanosheets decorated with superparamagnetic $CoFe_2O_4$ nanocrystals and their application as an enhanced electromagnetic wave absorber, RSC Advances 4 (2014) 33619-33625.

[24] Y.L. Ren, C.L. Zhu, L.H. Qi, H. Cao, Y.J. Chen, Growth of γ-Fe_2O_3 nanosheet arrays on graphene for electromagnetic absorption applications, RSC Advances 4 (2014) 21510-21516.

[25] M. Fu, Q.Z. Jiao, Y. Zhao, Preparation of $NiFe_2O_4$ nanorod-graphene composites via an ionic liquid assisted one-step hydrothermal approach and their microwave absorbing properties, Journal of Materials Chemistry A 1 (2013) 5577-5586.

[26] D.Z. Chen, H.Y. Quan, Z.N. Huang, S.L. Luo, X.B. Luo, F. Deng, H.L. Jiang, G.S. Zeng, Electromagnetic and microwave absorbing properties of RGO@ hematite core–shell nanostructure/PVDF composites, Composites Science and Technology 102 (2014) 126-131.

[27] X.J. Zhang, G.S. Wang, W.Q. Cao, et al. Enhanced microwave absorption property of reduced graphene oxide (RGO)-$MnFe_2O_4$ nanocomposites and polyvinylidene fluoride, ACS applied materials & interfaces 6 (2014) 7471-7478.

[28] M. Mahmoodi, M. Arjmand, U. Sundararaj, S. Park, The electrical conductivity and electromagnetic interference shielding of injection molded multi-walled carbon nanotube/polystyrene composites, Carbon 50 (2012) 1455-1464.

[29] V.H. Pham, T.V. Cuong, T.T. Dang, et al. Superior conductive polystyrene-chemically converted graphene nanocomposite, Journal of materials chemistry 21 (2011) 11312-11316.

[30] Z.P. Song, T. Xu, M.L. Gordin, et al. Polymer-graphene nanocomposites as ultrafast-charge and-discharge cathodes for rechargeable lithium batteries, Nano letters 12 (2012) 2205-2211.

[31] A.Y.W. Sham, S.M. Notley, A review of fundamental properties and applications of polymer-graphene hybrid materials, Soft Matter 9 (2013) 6645-6653.

[32] J.R. Potts, D.R. Dreyer, C.W. Bielawski, et al. Graphene-based polymer nanocomposites, Polymer 52 (2011) 5-25.

[33] V. Alzari, V. Sanna, S. Biccai, et al. Tailoring the physical properties of nanocomposite films by the insertion of graphene and other nanoparticles, Composites Part B: Engineering 60 (2014) 29-35.

[34] H. Kim, A.A. Abdala, C.W. Macosko, Graphene/polymer nanocomposites, Macromolecules, , 43 (2010) 6515-6530.

[35] F. Ren, G.M. Zhu, P.G. Ren, Y.K. Wang, X.P. Cui, In situ polymerization of graphene oxide and cyanate ester–epoxy with enhanced mechanical and thermal properties, Applied Surface Science 316 (2014) 549-557.

[36] W.K. Goertzen, M.R. Kessler, Dynamic mechanical analysis of fumed silica/cyanate ester nanocomposites, Composites Part A: Applied Science and Manufacturing 39 (2008) 761-768.

[37] H.J. Hwang, C.H. Li, C.S. Wang, Dielectric and thermal properties of dicyclopentadiene containing bismaleimide and cyanate ester. Part IV, Polymer 47 (2006) 1291-1299.

[38] C.H. Lin, Synthesis of novel phosphorus-containing cyanate esters and their curing reaction with epoxy resin, Polymer 45 (2004) 7911-7926.

[39] W.S. Hummers Jr, R.E. Offeman, Preparation of graphitic oxide, Journal of the American Chemical Society 80 (1958) 1339-1339.

[40] X.H. Li, H. Zhu, J. Feng, J.W. Zhang, X. Deng, B.F. Zhou, H.L. Zhang, D.S. Xue, F.S. Li, N.J. Mellors, One-pot polylol synthesis of graphene decorated with size-and density-tunable

Fe_3O_4 nanoparticles for porcine pancreatic lipase immobilization, Carbon 60 (2013) 488-497.

[41] Y.W. Cao, J.C. Feng, P.Y. Wu, Preparation of organically dispersible graphene nanosheet powders through a lyophilization method and their poly (lactic acid) composites, Carbon 48 (2010) 3834-3839.

[42] M.J. McAllister, J.L. Li, D.H. Adamson, H.C. Schniepp, A.A. Abdala, J. Liu, M. Herrera-Alonso, D.L. Milius, R. Car, R.K. Prud'homme, Single sheet functionalized graphene by oxidation and thermal expansion of graphite, Chemistry of Materials 19 (2007) 4396-4404.

[43] A.V. Murugan, T. Muraliganth, A.Manthiram, Rapid, facile microwave-solvothermal synthesis of graphene nanosheets and their polyaniline nanocomposites for energy strorage, Chemistry of Materials 21(2009) 5004-5006.

[44] X.A. Fan, J.G. Guan, X.F. Cao, W. Wang, F.Z. Mou, Low-Temperature Synthesis, Magnetic and Microwave Electromagnetic Properties of Substoichiometric Spinel Cobalt Ferrite Octahedra, European Journal of Inorganic Chemistry 2010 3 (2010) 419-426.

[45] Y.C. Qing, W.C. Zhou, F. Luo, D.M. Zhu, Epoxy-silicone filled with multi-walled carbon nanotubes and carbonyl iron particles as a microwave absorber, Carbon 48 (2010) 4074-4080.

[46] Y.C. Qing, D.D. Min, Y.Y. Zhou, F. Luo, W.C. Zhou, Graphene nanosheets and flake carbonyl iron particles filled epoxy−silicone composites as thin thickness and wide bandwidth microwave absorber, Carbon 86 (2015) 98-107.

[47] A. Paul, S. Thomas, Electrical properties of natural-fiber-reinforced low density polyethylene composites: A comparison with carbon black and glass-fiber-filled low density

polyethylene composites, Journal of applied polymer science 63 (1997) 247-266.

[48] K.S. Moon, H.D. Choi, A.K. Lee, K.Y. Cho, H.G. Yoon, K.S. Suh, Dielectric properties of epoxy-dielectrics-carbon black composite for phantom materials at radio frequencies, Journal of applied polymer science 77 (2000) 1294-1302.

[49] F. He, S. Lau, H.L. Chan, J.T. Fan High dielectric permittivity and low percolation threshold in nanocomposites based on poly (vinylidene fluoride) and exfoliated graphite nanoplates, Advanced Materials 21(2009) 710-715.

[50] G.S. Wang, X.J. Zhang, Y.Z. Wei, S. He, L. Guo, M.S. Cao, Polymer composites with enhanced wave absorption properties based on modified graphite and polyvinylidene fluoride, Journal of Materials Chemistry A 1(2013) 7031-7036.

[51] S.K. Pillalamarri, F.D. Blum, A.T. Tokuhiro, M.F. Bertino, One-pot synthesis of polyaniline-metal nanocomposites, Chemistry of materials 17 (2005) 5941-5944.

[52] H.Y. Liu, Y. Shen, Y. Song, C.W. Nan, Y.H. Lin, X.P. Yang, Carbon nanotube array/polymer core/shell structured composites with high dielectric permittivity, low dielectric loss, and large energy density, Advanced Materials 23 (2011) 5104-5108.

[53] X.J. Zhang, G.S. Wang, Y.Z. Wei, L. Guo, M.S. Cao, Polymer-composite with high dielectric constant and enhanced absorption properties based on graphene-CuS nanocomposites and polyvinylidene fluoride, Journal of Materials Chemistry A 1 (2013) 12115-12122.

[54] C. Wang, X.J. Han, P. Xu, X.L. Zhang, Y.C. Du, S.R. Hu, J.Y. Wang, X.H. Wang, The electromagnetic property of chemically reduced graphene oxide and its application as microwave absorbing material, Applied Physics Letters 98 (2011) 072906.